THE FOLDING KINETICS OF RIBONUCLEASE Sa AND A CHARGE-REVERSAL VARIANT

A Thesis

by

JARED MATTHEW TREFETHEN

Submitted to the Office of Graduate Studies of
Texas A&M University
in partial fulfillment of the requirements for the degree of

MASTER OF SCIENCE

December 2004

Major Subject: Biochemistry

THE FOLDING KINETICS OF RIBONUCLEASE Sa AND A CHARGE-REVERSAL VARIANT

A Thesis

by

JARED MATTHEW TREFETHEN

Submitted to Texas A&M University
in partial fulfillment of the requirements
for the degree of

MASTER OF SCIENCE

Approved as to style and content by:

_____	_____
C. Nick Pace (Chair of Committee)	David H. Russell (Member)
_____	_____
J. Martin Scholtz (Member)	Gregory D. Reinhart (Head of Department)

December 2004

Major Subject: Biochemistry

ABSTRACT

The Folding Kinetics of Ribonuclease Sa and a Charge-Reversal Variant.

(December 2004)

Jared Matthew Trefethen, B.S., University of California, Los Angeles

Chair of Advisory Committee: Dr. C. Nick Pace

The primary objective was to study the kinetics of folding of RNase Sa. Wild-type RNase Sa does not contain tryptophan. A tryptophan was substituted at residue 81 (WT*) to allow fluorescence spectroscopy to be used to monitor folding. This tryptophan mutation did not change the stability. An analysis of the folding kinetics of RNase Sa showed two folding phases, indicating the presence of an intermediate and consistent with the following mechanism: D ⇔ I ⇔ N. Both refolding limbs of the chevron plot (abcissa = final conc. of denaturant and ordinate = kinetic rate) had non-zero slopes suggesting that proline isomerization was not rate-limiting.

The conformational stability of a charge-reversed variant, WT*(D17R), of a surface exposed residue on RNase Sa has been studied by equilibrium techniques. This mutant with a single amino acid charge reversal of a surface exposed residue resulted in decreased stability. Calculations using Coulomb's Law suggested that favorable electrostatic interactions in the denatured state were the cause for the decreased stability for the charge-reversed variant. Folding and unfolding kinetic studies were designed and conducted to study the

charge-reversal effect. Unfolding kinetics showed a 10-fold increase in the unfolding rate constant for WT*(D17R) over WT* and no difference in the rate of refolding.

Kinetics experiments were also conducted at pH 3 where protonation of Asp17 (charge reversal site) would be expected to negate the observed kinetic effect. At pH 3 the kinetics of unfolding of WT* RNase Sa and the WT*(D17R) mutant were more similar. These kinetic results indicate that a single-site charge reversal lowered the free energy of the denatured state as suspected. Additionally, the results showed that the transition state was stabilized as well. These results show that a specific Coulombic interaction lowered the free energy in the denatured and transition state of the charge-reversal mutant, more than in WT*. To our knowledge, this is the first demonstration that a favorable electrostatic interaction in the denatured state ensemble has been shown to influence the unfolding kinetics of a protein.

DEDICATION

To my beloved wife, Emily, and to my beautiful daughters, Madeline, and Naomi: for their undying love, patience, and support through this process.

ACKNOWLEDGMENTS

In an effort such as this, I must first acknowledge those to whom I have dedicated not only this work but also my life: my family. I could not have done it without them by my side with constant encouragement and their consistent blessing. I want to thank Dr. Nick Pace for providing me with a project and a mentor. I want to acknowledge Dr. Marty Scholtz for always having his door open for questions and answers. I want to thank the Pace and Scholtz Labs for helpful discussions and training; I had to learn how to do it somewhere. I especially want to thank with all of my heart the time, effort, and dedication that Dr. David Brems invested in guiding me, teaching me and discussing my project. I could not have done it without his careful support and example. His vast experience in protein folding has proven to be an invaluable resource in making this project such a success. To all others that I have not mentioned, you are greatly appreciated.

TABLE OF CONTENTS

Page

LIST OF FIGURES

LIST OF TABLES

INTRODUCTION

Much is known about the structure and function of folded proteins. To ensure survival, an organism needs to process food to sustain life. A large part of the processing requires folded functional proteins. Most proteins are folded under physiological conditions into a functional form to fulfill their assigned role. However, the mechanism by which a protein folds into its unique conformation is not well understood. Anfinsen (Anfinsen 1973) showed that the sequence of a protein determines the folded 3D structure. This observation is important but has not helped us predict the 3D structure or to predict the mechanism of folding given just the amino acid sequence. If the folding of a small protein involved randomly searching all possible conformations, the process would take longer than the age of the universe (Daggett and Fersht 2003), hence the Levinthal paradox (Levinthal 1969). Research has shown that unfolded proteins rapidly collapse into condensed states and populate transient intermediary states during folding. These transient folding states decrease the number of possible conformations, limit the search for possible conformations, and help guide the folding process to the native state. However, the characterization of these intermediate folding states has been difficult, so we still have a poor understanding of the mechanism of protein folding.

Another significant problem in understanding protein folding is our inability to predict the 3D structure given the amino acid sequence and determining the contribution of the forces involved in stabilizing the 3D structure. Such forces

---

This thesis follows the style of *Biochemistry*.

include hydrogen bonding, electrostatic interactions, van der Waals forces, and the hydrophobic effect. Each of these forces on an individual basis is relatively weak, although, collectively, they are significant. For example, the difference in free energy between the folded and unfolded states is the difference in the sum of the forces that contribute to the folded and unfolded structures. Moreover, the major force that favors the unfolded state is entropy. In most proteins, the difference in free energy between the native and denatured states is small. Furthermore, the contribution of each factor alone or the collective contribution thereof for each protein is not known and is a major problem in the protein folding field.

The Denatured State

In folding, a protein starts out in a highly unfolded, denatured state and proceeds to a uniquely folded native state. The denatured state is a large ensemble of conformations interconverting at a rapid rate. In the past, the denatured state was thought to be devoid of intramolecular interactions, such that a protein's stability could be explained mainly in terms of interactions in the native state. However, in recent years, it has become apparent that many proteins contain residual structure in the denatured state (Fersht 2000; Kazmirski et al. 2001) and are more compact than earlier data had suggested.

The denatured states of proteins are important in determining the stability of a protein, since stability is defined as the difference in free energy between the native and denatured states. The native state of a protein has a relatively well-

defined set of atomic interactions, but the denatured states do not. In cells, tissues, and physiological solutions, the native states are in dynamic equilibrium with the denatured conformations. Theory and experiments indicate that the denatured state should be viewed as a distribution of many microstates that change with the conditions of solution and depend on the protein sequence.

For many years, protein chemists thought that the denatured state approached a random coil conformation (Tanford et al. 1966). However, investigations over the past two decades have provided ample evidence that the denatured state may have limited amounts of structure (Dill and Shortle 1991). Many of the techniques designed to study protein structure have provided information about the nature of the unfolded state. X-ray crystallography and NMR spectroscopy are techniques that have provided structural data at the atomic level for the native state. However, since the denatured state is a collection of microstates, a single crystal structure or a view averaged by NMR spectroscopy is still incomplete due to the inherent flexibility of the members of the denatured state ensemble. The study described in this work involves the preliminary development of the folding mechanism of RNase Sa. Additionally, information on the effect of a charge-reversed, surface exposed residue on the unfolded state of RNase Sa (Pace et al. 2000) is provided.

Protein Stability

To understand protein stability, the critical interactions that determine the different conformational states must be characterized. Changes in these

interactions can either increase or decrease the stability of the protein. Some studies have examined the effect of the loss of a key interaction, and others have studied the effect of an added interaction. For example, if an electrostatic interaction is introduced into a protein, it will generally affect the stability of that protein. Grimsley et al. (Grimsley et al. 1999) showed that reversing the charge on the side chain of a surface exposed amino acid residue in RNase Sa could lead to increased or decreased stability (Pace et al. 2000). Coulomb's Law predicted an increase in stability in each case studied, if the denatured state was assumed not to contribute. However, one of these charge-reversal mutants, D17K, showed a decrease in stability. This suggested that the free energy of the denatured state might have decreased more than that of the native state when the charge of the side chain is reversed. Therefore, they reasoned that the electrostatic interaction introduced by the charge-reversal was more significant in the denatured state and favorable Coulombic interactions might be important in determining the denatured state ensemble.

Kinetic folding and unfolding studies coupled with previous equilibrium data of RNase Sa and a charge-reversal variant of RNase Sa may help to better understand the effect of such a charge-reversed side chain on the denatured state ensemble and protein folding. Kinetic studies have the potential to demonstrate the direct consequence of a charge-reversed side chain on the denatured state as suggested by the equilibrium data. Folding and unfolding rates determined by kinetics can also identify a change in stability of the transition state(s). Joining the power of kinetics with equilibrium studies is the

key to clearly identifying the effect of a point mutation (Matthews 1987) on a globular protein such as RNase Sa.

Frequently a two-state model, D ⇔ N, where D is the denatured or unfolded state and N is the native state has been sufficient for analyzing equilibrium studies. The free energy of a protein folding reaction at equilibrium is defined as the ratio of the concentrations of N and D at equilibrium

$$D \leftrightarrow N \tag{1}$$

where *D* is the denatured state and *N* is the native state. Additional insight into the folding reaction can be gained by determining the folding and unfolding rate constants. They can be combined to a ratio that is equal to the equilibrium constant, K_{eq}, as shown below,

$$K_{eq} = \left[N\right] / \left[D\right] \tag{2}$$

where *N* is the population of the natively folded protein and *D* is the population of the protein that is denatured. This can also be derived from the ratio of the folding and unfolding rate constants

$$K_{eq} = k_f / k_u \tag{3}$$

where k_f and k_u are the rate constants of folding and unfolding, respectively. The equilibrium constant allows one to solve for the standard free energy change, $\Delta G°$, as shown in

$$\Delta G^\circ = -RT \ln \left[N\right] / \left[D\right] = -RT \ln K_{eq} \quad (4)$$

where R is the gas constant (1.987 cal mol^{-1} K^{-1}). If, upon mutation of a residue, the overall stability changes, the difference is represented by

$$\Delta\Delta G = \Delta G_{mut} - \Delta G_{wt} \quad (5)$$

Figure 1 shows that the stability of a variant (*mut*) of the protein can be either larger or smaller than that of the wild-type (*wt*).

The two-state model assumes no significant concentration of intermediate present at equilibrium. Proteins that do exhibit an observable intermediate(s) are considered to follow a three-state or higher-state model ($D \leftrightarrow I_n \leftrightarrow N$), where n is the number of intermediates observed.

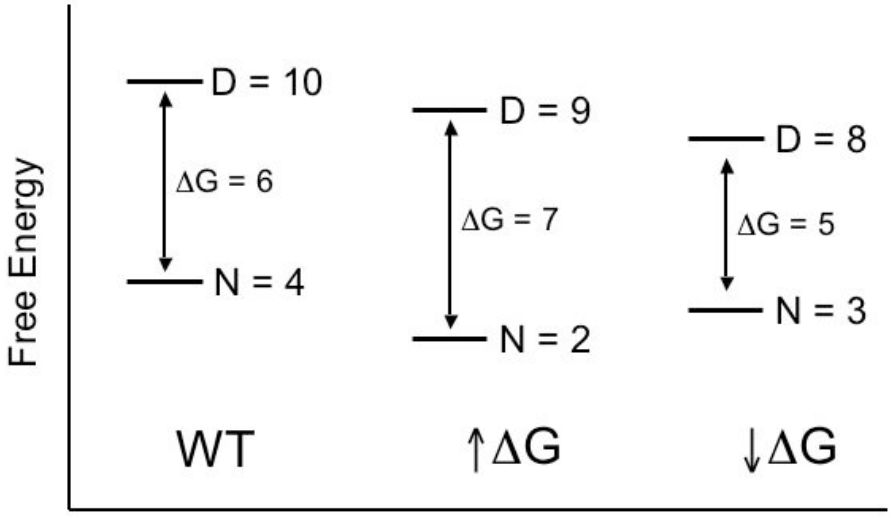

FIGURE 1: Free energy model representing an increase and decrease in conformational stability as a result of an effect on either the native state (N) and/or the denatured state (D).

Kinetic Analysis

Equilibrium studies characterize differences in the structure and stability of the native and denatured states of a protein. Such equilibrium studies are important in characterizing a given protein and have provided definitive information about proteins at equilibrium. However, a better understanding of the mechanism of folding often can be gained from kinetic studies of protein folding. Often transient intermediate states are observed in kinetic folding studies that may not be present at equilibrium.

The information gleaned from kinetic experiments complement and build upon the information obtained from equilibrium studies in order to create a model of the folding pathway. Equilibrium studies provide the basis for stabilities along a reaction coordinate. This is represented by a shift in either melting temperature, or lability of the protein's folded structure to the presence of a

chaotropic agent, such as urea. If a change in the protein's structure results in an observed difference in stability, it is not possible from equilibrium measurements to know which state has been affected. By measuring the rates at which folding or unfolding occur from the denatured or native state, respectively, the nature of the effect of a point mutation on the denatured state, native state, any intermediary states, and transition states can be surmised. The rate limiting transition state may be mapped out and characterized only by kinetic approaches. Additionally, equilibrium studies do not tell us anything about folding rates. Due to the nature of equilibrium conditions, there is no time parameter involved in equilibrium experiments. An equilibrium denaturation curve may show two-state behavior whereas kinetic studies may demonstrate more complicated behavior. Equilibrium measurements require sufficient denaturant to perturb the native state such that less stable forms, intermediates, or denatured states are populated. Kinetic folding experiments monitor states that are less stable than the native state in solvent conditions that strongly promote structure.

To build the immense library of knowledge of protein folding, a number of model proteins have been used to investigate the mechanisms of two-state folding (T4 lysozyme) (Chen et al. 1992), folding of proteins with intermediary states (barnase, ribonuclease T1, chymotrypsin inhibitor 2, cytochrome c, etc.) (Serrano et al. 1992; Mayr et al. 1993b; Matouschek et al. 1994; Hebert et al. 1998; Akiyama et al. 2000; Fersht 2000; Wong et al. 2000; Yeh and Rousseau 2000; Kazmirski et al. 2001; Hoang et al. 2002; Daggett and Fersht 2003; Khan

et al. 2003), and the effects of reversed charges and other mutations on folding (ribonuclease Sa, staphylococcal nuclease, lysozyme, etc.) (Hebert et al. 1998; Pace et al. 1998; Pace et al. 2001; Shaw et al. 2001; Ilinskaya et al. 2002; Laurents et al. 2003; Yakovlev et al. 2003; Alston 2004). These proteins are some of the well-studied models of protein folding and have yielded a large amount of knowledge that continues to drive the investigation of how proteins fold. The protein used in this study is RNase Sa, which has been extensively studied at the equilibrium level. Here, I report studies of the folding kinetics of RNase Sa, which have never before been published. Insight into the folding mechanism of RNase Sa may be gained from studies of related ribonucleases, such as ribonucleases T1 and Ba.

Folding Kinetics of Related Ribonucleases (T1 and Ba)

Nucleases are a class of hydrolytic enzymes that catalyze the cleavage of both DNA (DNases) and/or RNA (RNases). The two best-characterized families of RNases are the mammalian RNases and the microbial RNases. The mammalian RNases, represented by RNase A, are the fastest evolving family of proteins (Rosenburg et al. 1995). These include RNases such as angiogenin, which stimulates blood vessel development, and onconase, which is being developed for cancer treatment. In the microbial family, RNase T1 was the first to be identified. Originally this eukaryotic ribonuclease was found in the culture medium of the fungus *Aspergillus oryzae*, which is used in the fermentation of sake and the production of soy sauce. RNase Ba (Barnase) from *Bacillus*

amyloliquifaciens was the first prokaryotic ribonuclease to be identified and purified (Pace et al. 1998). For years it has been widely studied as a model for protein folding (Daggett and Fersht 2003).

The Schmid Lab has studied RNase T1 extensively and RNase Ba (barnase) has been explored by the Fersht lab. Ribonucleases Sa, T1 and Ba have limited sequence identity (Figure 2). All three are composed of secondary $\alpha+\beta$ structures. RNases Sa, Ba, and T1 have remarkably similar structures in the β-sheet regions near the active sites, but there are substantial differences in the α-helices and turns (Figure 3; (Pace et al. 1998)).

```
Sa                                                  D V S G T V C L S A L    11
Ba    A Q V I N T F D G V A D Y L Q T Y H K L P N D Y I T K S E A Q A    32
T1                              A C D Y T C G S N C Y S S   S D V S T    18

Sa    P P E A T [D] T L N L I A S D G P F P Y S Q D G V V F Q N R E S V    43
Ba    L G W V A S K G N L A D V A   P G   K S I G G D I F S N R E G K    62
T1        A Q A A G Y Q L H E D G E T V G S N S Y P H K Y N N Y E G F    48

Sa    L P T Q S Y G Y Y H E Y T V             I T P G A R T R G T R R    69
Ba    L P G K S G R T W R E A D I           N Y T S G F     R N S D R    87
T1    D F S V S S P   Y Y E W P I L S S G D V Y S G G S P     G A D R    77

Sa    I I T G E A T Q E D Y [Y] T G D H Y A         T F S L I D Q T C      96
Ba    I L Y S S D W   L I Y K T T D H Y Q         T F T K I R           110
T1    V V F N E N N   Q L A G V I T H T G A S G N N F V E C T           104
```

FIGURE 2: Sequence alignment of RNase Sa, Ba and T1. Position 17 and position 81, shown in boxes, are the sites of mutations for a charge-reversal (WT*(D17R)) and a probe (Y81W) to facilitate fluorescence studies. Adapted from refs. (Hill et al. 1983; Hebert et al. 1997; Alston 2004).

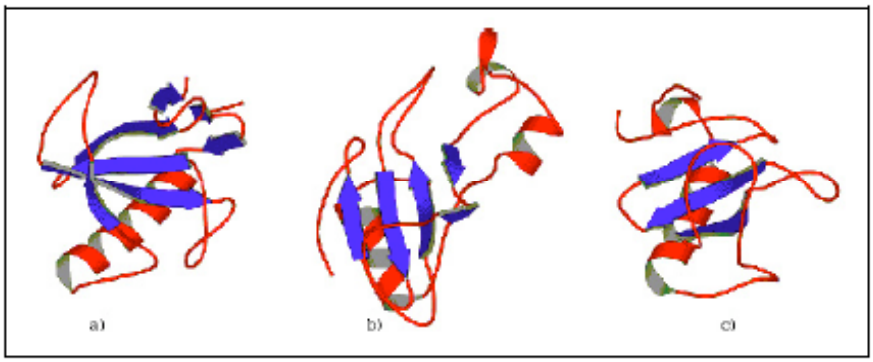

RNase	Seq. ID
Sa	100 %
Ba	23 %
T1	11 %

FIGURE 3: Structural comparison of related ribonucleases. Left, Secondary structures of a) RNase T1, b) RNase Ba (barnase), and c) RNase Sa. This plot was prepared using the program MOLSCRIPT (Kraulis 1991). Right, sequence identity of the three ribonucleases (adapted from refs. (Pace et al. 1998; Alston 2004)

RNase T1 is a small protein of 104 residues (4 proline residues) and has been used as a model for studying the mechanism of protein folding. Like RNase Sa, T1 exhibits two-state folding under equilibrium conditions. However, kinetic studies show that the folding pathway is more complicated (Mayr et al. 1996). Two of the four prolines are in the *cis* conformation in the native state and give rise to slow unfolding steps. A hallmark of folding reactions limited by proline isomerization is an independence of their rate on denaturant concentration. Variants of RNase T1, where the *cis* prolines were replaced by other amino acids, eliminated the slow step of folding (Mayr and Schmid 1993b; Mayr et al. 1996), showing that the slow step was due to proline isomerization.

Barnase is a 110-residue protein with three proline residues and has also been used as a model for studies of the mechanism of protein folding. Early studies observed only one intermediate (I ⇔ N) in the folding mechanism of barnase, which led to the suggestion of a three-state model. This three-state

reaction was affirmed by identifying a kinetically significant on-pathway intermediate (Fersht 2000). Later, data have revealed a more complicated mechanism. First, a rapid folding step from the unfolded to the first intermediate is observed ($t_{1/2} \approx 200\mu s$), followed by the formation of a second intermediate ($t_{1/2} \approx 60ms$) that is highly native-like ($I_1 \leftrightarrow I_2 \leftrightarrow N$). From the native-like intermediate, *trans* ↔ *cis* isomerization of the peptidyl-Pro48 bond occurs on the time scale of minutes to give the final native structure (Fersht 1999).

RNase Sa has 6 prolines (Figure1) and they are all trans in the native state. Based on previous refolding experiments (unpublished data), RNase Sa, like RNase T1 and Ba, showed evidence of multiple phases at low denaturant concentration. This has been verified and further details concerning the folding pathway were gained in this project.

Ribonuclease Sa

Ribonuclease Sa (RNase Sa) is the smallest member of the family of microbial ribonuclease family and is the model protein used in this study. RNase Sa is an acidic protein (pI = 3.5; net charge of -7 at pH 7) of 96 amino acid residues (MW = 10575) from S*treptomyces aureofaciens*. S*. aureofaciens* is used in the production of chlortetracycline (Pace et al. 1998), an antibiotic used in the treatment of Chlamydia and general eye infections (Rang et al. 2001). *S. aureofaciens* secretes ribonucleases into the extracellular medium. Three of these have been previously characterized: RNase Sa from strain BMK, RNase Sa2 from strain R8/26, and RNase Sa3 from strain CCM 3239 (Pace et al. 1998).

Native crystal structures of RNase Sa have been determined at resolutions of 1.8Å (Sevcik et al. 1991), 1.2Å (Sevcik et al. 1996), and 1.0Å (Sevcik et al. 2002). Additional structures have been determined with nucleotides bound (Sevcik et al. 1990; Sevcik et al. 1991; Sevcik et al. 1993a; Sevcik et al. 1993b) and for variants (Schell 2003).

The native state of proteins is stabilized by several forces. Electrostatic interactions, van der Waals forces, hydrogen bonding, and hydrophobic effects contribute to the stabilization of a protein. Considering the collection of forces, removing a favorable electrostatic interaction would be expected to reduce the stability of the protein. Alternatively, if a favorable electrostatic interaction is engineered into a protein, a stability increase might be expected. A previous study (Pace et al. 2000) of RNase Sa presumed that if a favorable electrostatic interaction was introduced into RNase Sa by reversing the charge of one or more negatively-charged side chains that were surface exposed and in close proximity to other negative charges, an increase in stability should be achieved. Based on Coulomb's Law, the charge-reversal mutants were expected to be more stable if there were no specific interactions in the denatured state. However, the stability increase was not as large as predicted by Coulomb's Law and, surprisingly, one of the charge-reversal variants, D17K, showed a decrease in stability of approximately 1.1 kcal/mol. This led to the idea that specific electrostatic interactions are more significant in the denatured state ensemble than in the native state. Appropriately, the hypothesis that followed was that long-range electrostatic interactions are important in determining the makeup of the

denatured state ensemble and play an important role in the mechanism of protein folding (Pace et al. 2000). In this study, the folding kinetics of RNase Sa were determined. In addition, information was obtained with regard to the effect of the charge-reversal on the folding behavior of RNase Sa at neutral pH and pH 3.

These experiments were performed by following changes in the fluorescence of a variant of RNase Sa in which a tryptophan residue replaced a tyrosine at position 81. This tryptophan mutation did not change the stability. Wild-type RNase Sa has 8 tyrosine residues and no tryptophan residues (Figure 2). Folding could not be followed by tyrosine fluorescence with WT RNase Sa because the difference in fluorescence intensity between the native and denatured states was too small (unpublished results). Therefore, the tryptophan substitution was utilized to improve our ability to follow the folding of RNase Sa.

The Effects of pH on Protein Folding

The consequence of the charge-reversal on folding kinetics was explored further by varying the pH of the folding experiment. In addition to temperature and chemical denaturants, salts and pH variations can effect denaturation as well. The pH alters the ionization of amino acid side chains, which changes protein charge distributions and hydrogen bonding requirements. At low pH, for example, the ionizable groups are protonated and positive charges abound in comparison to their negative counterparts. Therefore, it might be expected that the rate constants for refolding will be significantly altered at low pH.

RESULTS

Equilibrium Analysis

We set out to determine the folding kinetics of RNase Sa in a tryptophan background (Y81W) and a charge reversal variant (Y81W/D17R). Throughout this work Y81W RNase Sa will be referred to as WT* and the charge-reversal variant will be appropriately named WT*(D17R). The location of the tryptophan insert proved to be an excellent choice as evidenced by a large change in fluorescence intensity (2.5X) between the native and denatured state (Figure 4). The native state has a λ_{max} at 319nm while the denatured state displays a red shift of 22 nm and quenched fluorescence (λ_{max} = 341nm). Equilibrium folding experiments on both species of RNase Sa have already been published (Pace et al. 1998; Alston 1999; Grimsley et al. 1999). However, we repeated them using fluorescence spectroscopy at a much lower protein concentration than before.

At pH 7, RNase Sa is negatively charged. There is very little difference between the secondary structure in wild-type RNase Sa and its Y81W mutant as shown by circular dichroism (CD; Figure 5). WT* RNase Sa was as stable as its

wild-type counterpart with a midpoint of the urea denaturation curve (C_{mid}) at approximately 6M urea and was fully denatured at 8M urea. WT*(D17R), the charge-reversal mutant, showed a decrease in C_{mid} to 4.8M urea and was fully denatured at 7M urea (Figure 6). The change in stability, -1.1 kcal/mol, agreed with previously published data (Pace et al. 2000).

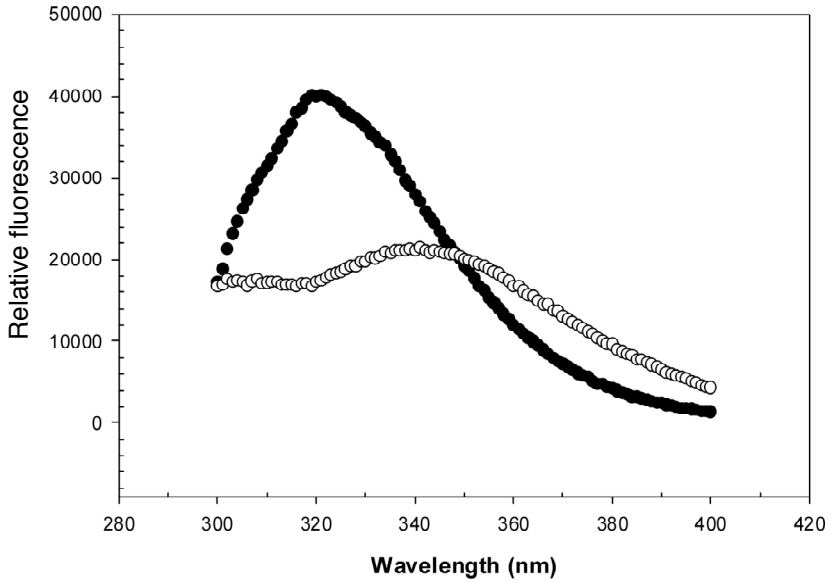

FIGURE 4: Emission spectra of native and denatured WT* RNase Sa. Excitation occurred at a wavelength of 278 nM ([protein] = ~0.94 mM) in 30 mM MOPS, pH 7.0, and 25 ^{o}C for the native (filled circles) and denatured (open circles) in 10 M urea, pH 7.0, and 25°C. The native λ_{max} is 319 nm, and the denatured λ_{max} is 341 nm using a 2 nm emission bandpass. Adapted from reference (Alston 2004).

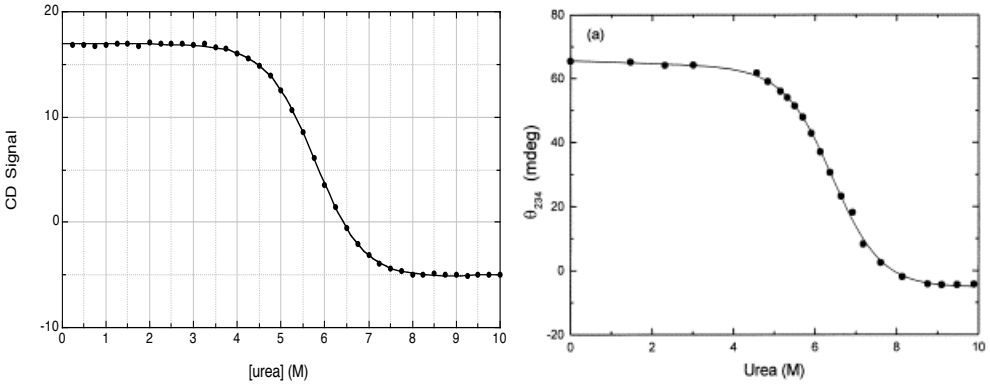

FIGURE 5: Urea denaturation curve of WT* RNase Sa and WT RNase Sa by circular dichroism. Left: Urea denaturation of WT* RNase Sa in the tryptophan background was at 25°C and pH 7 in 30mM MOPS. Circular dichroism was detected at 234nm. Right: urea denaturation curve of WT RNase Sa as measured under the same conditions as WT* in the tryptophan background. This figure was adapted from ref. (Pace et al. 1998).

To show that charge-reversal is the key element effecting RNase Sa stability, equilibrium folding experiments were carried out at pH 3. The denaturant *m*-value, which is the slope of the denaturation curve, is a measure of the effect of urea on ΔG of a protein (Pace and Scholtz 1997) and often increases as the pH is decreased. The *m*-value mainly reflects the change in hydrophobic surface area due to unfolding (Myers et al. 1995). Pace et al. (Pace et al. 2000) explained that the denatured state is expanded at low pH probably due to the high number of positive charges resulting in charge-charge repulsion and therefore, urea is able to interact with a larger surface area at low pH than at neutral pH. The pI of RNase Sa is approximately 3.5 and the pK of the side chain carboxyl group of Asp17 is 3.7 (Laurents et al. 2003). At pH 3, the side chain of Asp17 is 80% protonated, while the side chain of arginine at the same position in WT*(D17R) will remain positively charged. Protonation of the side chain of Asp17 decreases the probability of the formation of an electrostatic interaction

with a positive charge. Moreover, electrostatic interactions involving the positively charged arginine side chain in WT*(D17R) will be reduced because few amino acid side chains are negatively charged at pH 3. Thus, at pH 3 both WT* and WT*(D17R) RNase Sa should be similar. As expected at pH 3, WT* and WT*(D17R) were more similar (Figure 7) than at pH 7 and the stabilities of WT* and WT*(D17R) differed by only -0.3 kcal/mol (Table 1). The stabilities were decreased at pH 3 compared to stability values at pH 7. This is, perhaps, due to increased expansion throughout the denatured state by an excess of positive charges.

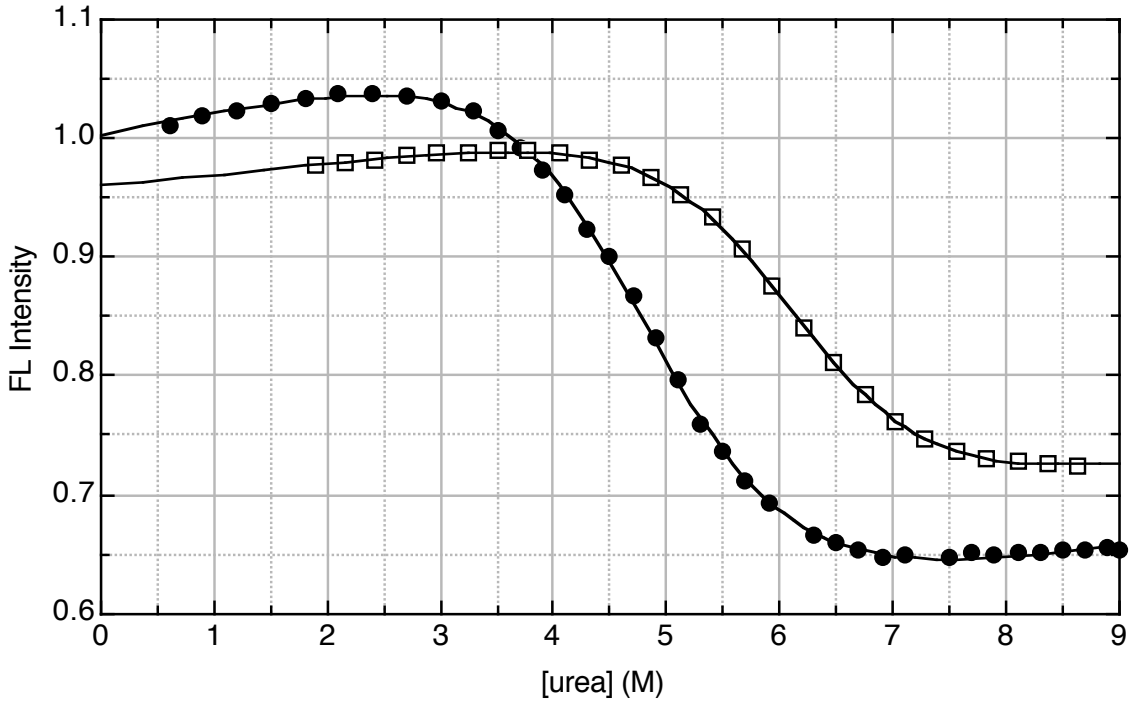

FIGURE 6: Urea denaturation curves of WT*(D17R) and WT* RNase Sa followed by fluorescence intensity at pH 7. The excitation wavelength was 280nm while emission was filtered by a 320nm cut-off filter at 25°C and pH 7 (30mM MOPS). Filled circles represent the equilibrium denaturation for WT*(D17R) RNase Sa. Open squares represent the equilibrium denaturation of WT* RNase Sa.

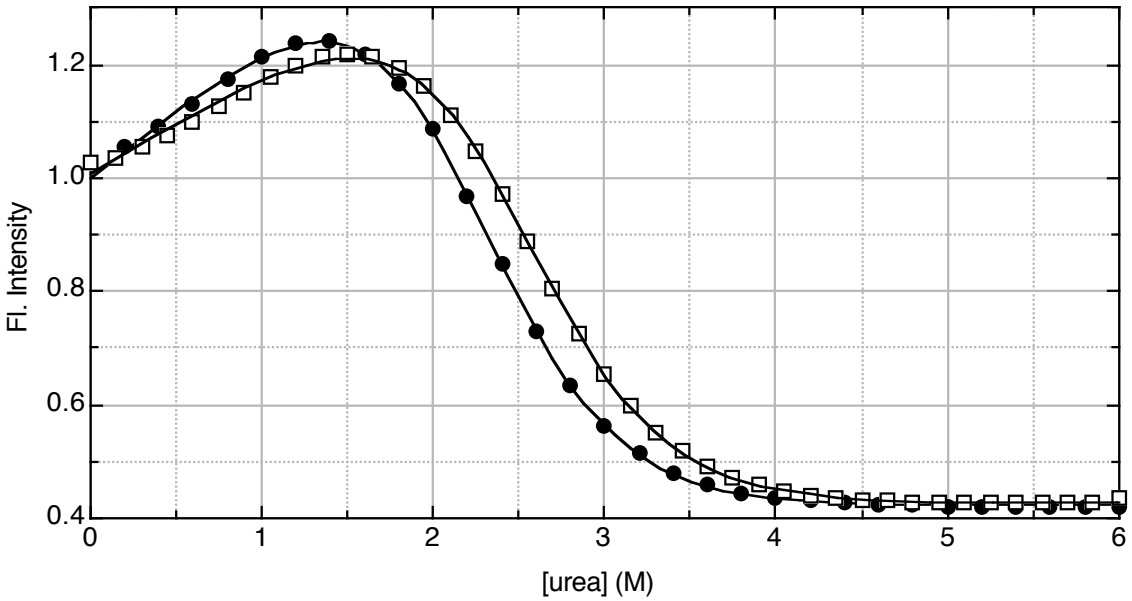

FIGURE 7: Urea denaturation curves of WT*(D17R) and WT* RNase Sa followed by fluorescence intensity at pH 3. The excitation wavelength was 280 nm while emission was filtered by a 320 nm cut-off filter at 25°C and pH 3 (30 mM glycine). Filled circles represent the equilibrium denaturation for WT*(D17R) RNase Sa. Open squares represent the equilibrium denaturation of WT* RNase Sa.

TABLE 1: Equilibrium stability results for WT* and WT*(D17R) RNase Sa at pH 3 and pH 7.

	Equilibrium			
	WT*(D17R)		WT*	
	pH 3	pH 7	pH 3	pH 7
m (cal/mol•M)	1600	955	1500	960
C_m (M)	2.12	4.84	2.43	6.01
$\Delta G(H_2O)$ (kcal/mol)	3.42	4.62	3.71	5.75

Kinetic Analysis

The refolding and unfolding kinetics of WT* and WT*(D17R) RNase Sa were performed at 25°C and at pH 7 and pH 3. Chevron plots were generated by plotting the natural logarithm of the observed rate constant against the final urea concentration. Refolding was accomplished by diluting a protein stock solution containing urea to allow refolding of the protein. Unfolding was accomplished by diluting a protein stock solution without urea to a final concentration of urea to cause unfolding. A typical refolding experiment at pH 7 done by a manual mixing technique is shown in Figure 8.

At pH 7, refolding rates at low urea concentrations were fitted to a biexponential rate equation. Multiexponential rate equations often indicate the presence of at least one stable, detectable intermediate. The unfolding limbs of the chevron plot (Figure 9) of WT* and WT*(D17R) RNase Sa were fitted to a single exponential equation, indicating the absence of an intermediate at high urea concentrations. Since the slopes of the refolding limbs were non-zero, it is very likely that the observed phases are not a result of a solvent-independent folding reaction such as proline isomerization.

The charge-reversal variant of RNase Sa showed refolding rates in close agreement with those of WT* RNase Sa with the indication of solvent-dependent intermediates present at low urea concentrations. The most notable difference was the unfolding rate constant for the charge-reversal variant, which was nearly 10 times faster (5.4×10^{-5} s^{-1}) than WT* (6.5×10^{-6} s^{-1}).

The amplitudes of WT* RNase Sa (Figure 10) showed that the slow reaction occupied a small percentage of the overall unfolding reaction from 0M to 2M urea. As the urea concentration increased, the amplitude of the slow reaction increased to ~100%.

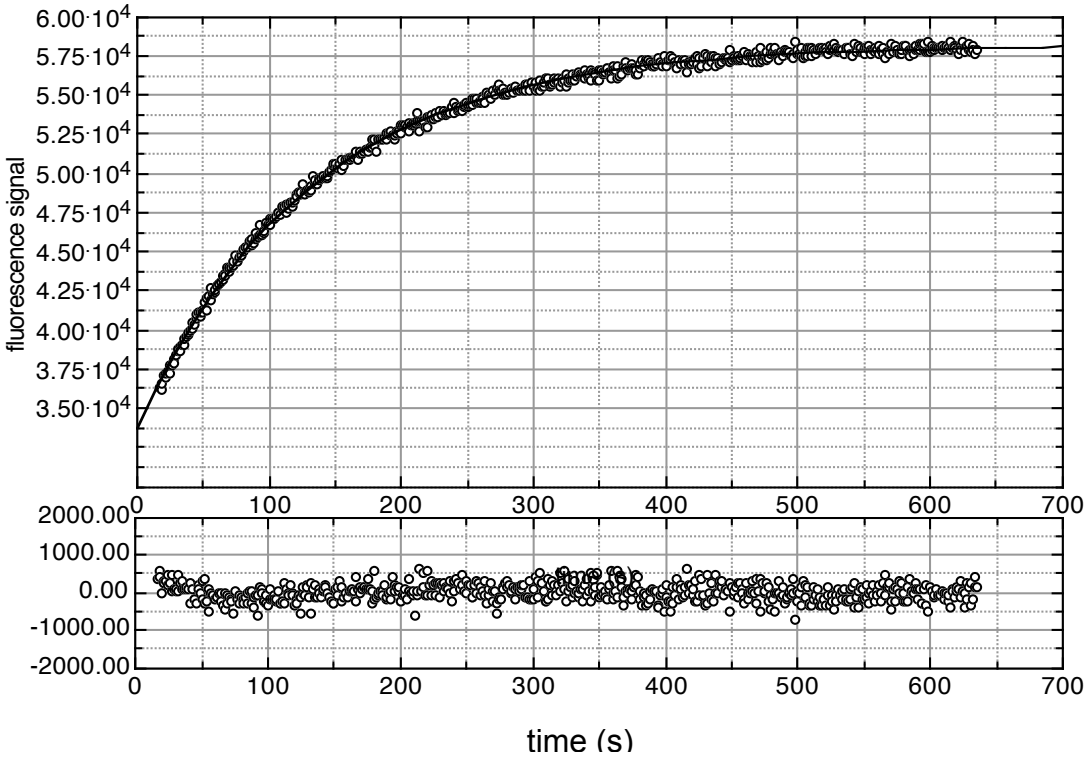

FIGURE 8: Refolding progress curve data of WT* RNase Sa as obtained by manual mixing at pH 7. Symbols represent data points and the line represents a curve of best fit to the data (see Mateials and Methods). The fit quality is represented by the residual data in the lower panel. See "Materials and Methods" for a complete experimental description: λ_{ex} = 280 nm; Emission monochromator was set at 319 nm (λ_{em} = 319 nm); [protein] = ~0.6 μM; final [urea] = 6.0 M at 25°C and pH 7 (30 mM MOPS).

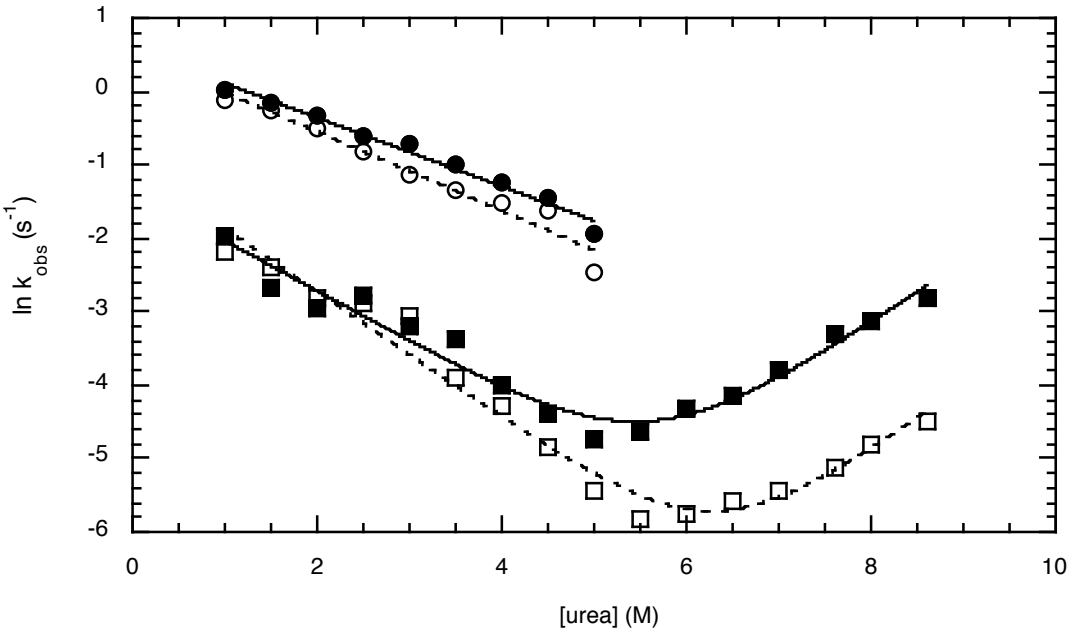

FIGURE 9: Chevron plot of WT* and WT*(D17R) RNase Sa refolding and unfolding at pH 7. Filled symbols correspond to WT*(D17R) RNase Sa. Open symbols correspond to WT* RNase Sa. Circles correspond to the fast refolding rates of both the charge-reversal and WT* RNase Sa. Squares represent the slow refolding and unfolding reactions of both proteins.

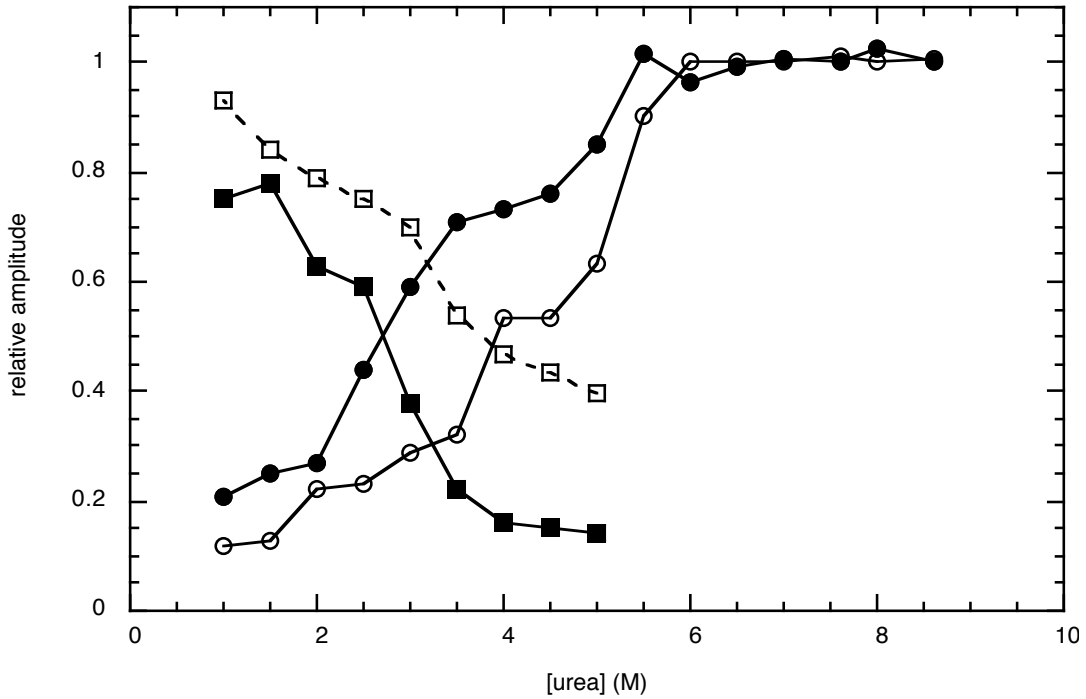

FIGURE 10: Relative refolding and unfolding reaction amplitudes of WT* and WT*(D17R) RNase Sa at pH 7. Filled symbols correspond to WT*(D17R) RNase Sa. Open symbols correspond to WT* RNase Sa. Circles correspond to the amplitudes of the fast refolding rates of both WT* and charge-reversal RNase Sa. Squares represent the amplitudes of the slow refolding and unfolding reactions of both proteins.

TABLE 2: Kinetic *m*-values and rate constants for WT* and WT*(D17R) RNase Sa at pH 7.

	***m*-values** (cal/mol•M)	***m*-values** (cal/mol•M)	**Rate constants** (s^{-1})		
	-equilibrium-	*-kinetics-*	k_f (fast)	k_f (slow)	k_u
WT*(D17R)	955	1030	1.8	0.26	5.4×10^{-05}
WT*	960	910	1.7	0.36	6.5×10^{-06}

Our hypothesis is that at pH 3, WT* and WT*(D17R) RNase Sa should be similar in terms of their folding kinetics, which is supported by stability studies done at equilibrium (Table 1). A typical unfolding progress curve at pH 3 is shown in Figure 11. Highly protonated WT* and WT*(D17R) RNase Sa have comparable folding and unfolding rates. Figure 12 shows that the fast folding and unfolding phases of both proteins have become more similar as the pH was decreased to 3. Moreover, the slow folding and unfolding phases are nearly identical. The corresponding amplitudes in Figure 13 support this finding. As urea concentration increased, the amount of each reaction corresponding to a particular phase (i.e. fast, slow, etc.) changed. WT* and WT*(D17R) showed very similar amplitude distributions as a function of urea. At pH 7 the difference in amplitude distributions between WT* and WT*(D17R) were clearly larger (Figure 10), as the native state of WT*(D17R) unfolded at lower denaturant than that of WT*. At pH 3 most electrostatic interactions are repulsive. Kinetic differences between WT* and WT*(D17R) decreased and were more similar. Even though the kinetics at pH 3 have proved to be more complicated than expected, the objective of overcoming the effect of the charge-reversal at low pH has been well illustrated. To further characterize the kinetics at pH 3, additional experiments should be performed.

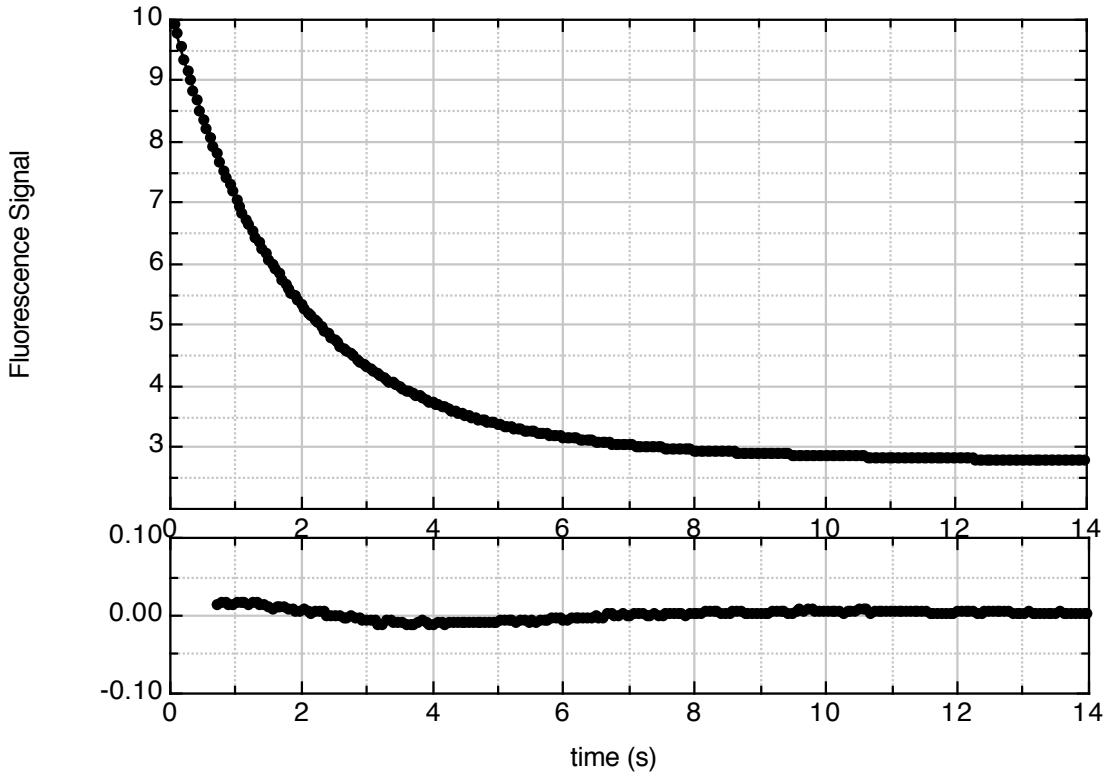

FIGURE 11: Unfolding progress curve data of WT*(D17R) RNase Sa as obtained by stopped-flow at pH 3. Symbols represent data points and the line represents a curve of best fit to the data (see Materials and Methods). The fit quality is represented by the residual data in the lower panel. See Materials and Methods for a complete experiment description: λ_{ex} = 280 nm; 305 nm cut-off filter was also used to capture 319 nm emission wavelength; [protein] = ~0.1 μM; final [urea] = 4.12 M at 25°C and pH 3 (30 mM glycine).

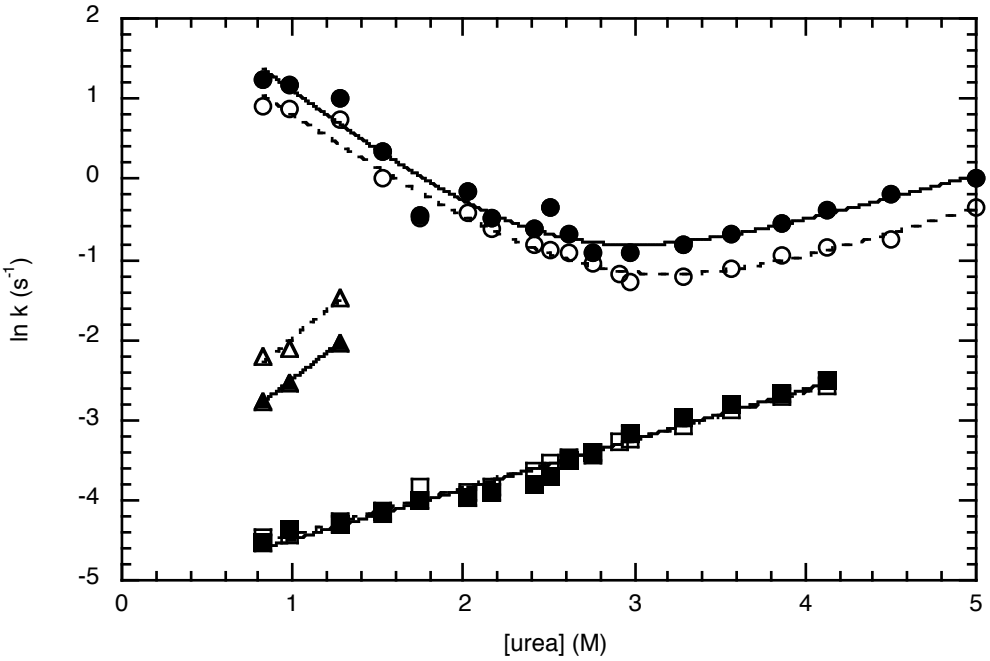

FIGURE 12: Chevron plot of WT* and WT*(D17R) RNase Sa refolding and unfolding at pH 3. Filled symbols correspond to WT*(D17R) RNase Sa. Open symbols correspond to WT* RNase Sa. Circles correspond to the fast rates of both WT* and WT*(D17R) RNase Sa, respectively. Triangles and squares correspond to the slower phases with the squares referring to the slowest phase.

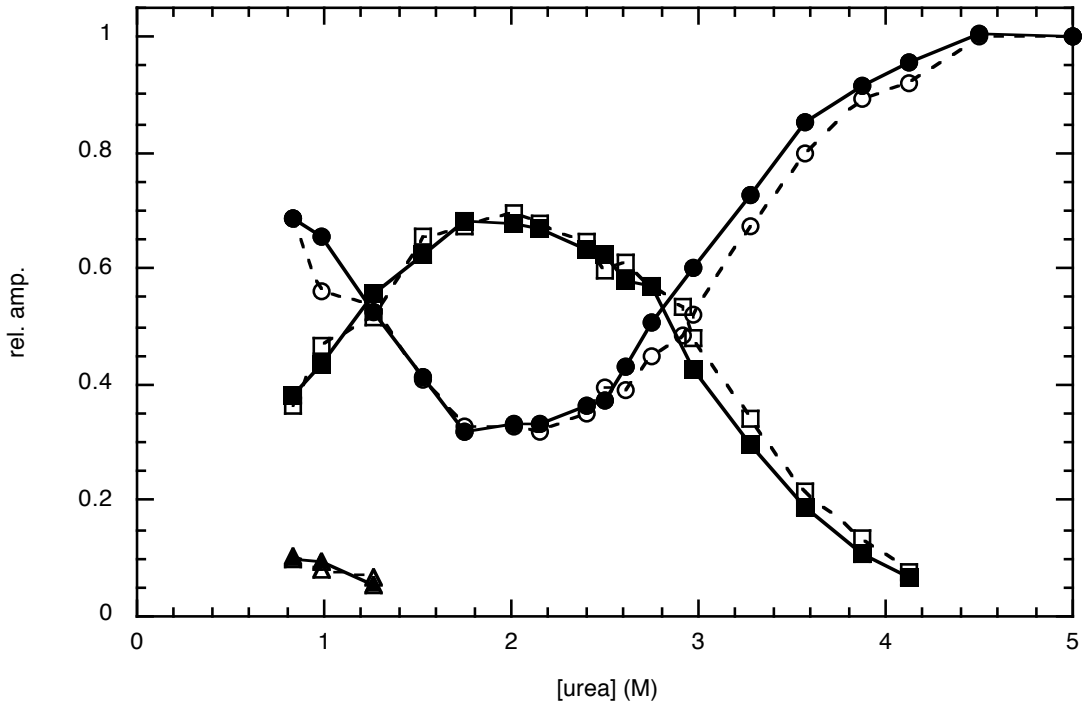

FIGURE 13: Relative refolding and unfolding reaction amplitudes of WT* and WT*(D17R) RNase Sa at pH 3. Filled symbols correspond to WT*(D17R) RNase Sa. Open symbols correspond to WT* RNase Sa. Circles correspond to the amplitudes of the fast rates. Squares and triangles represent the amplitudes of the slower phases with squares referring to the slowest phase.

DISCUSSION

Kinetic unfolding and refolding experiments were conducted for WT* and WT*(D17R) RNase Sa at 25°C at neutral and acidic pH. The kinetic curves were fit to first-order rate equations containing one or more exponential terms. Rate constants at each urea concentration were fit logarithmically to an equation showing a relationship between denaturant and the observed folding rate, to obtain chevron plots.

WT* refolding at pH 7 required two exponential terms to fit the data while unfolding required only one. The folding results are consistent with the presence of a stable intermediate at low denaturant concentrations, which was undetectable in unfolding experiments at higher denaturant concentrations. Evidence of a rate-limiting proline isomerization reaction was not seen under these conditions.

RNase T1 and barnase are close relatives of RNase Sa. T1 and barnase have multiple proline residues as does RNase Sa, which has six. T1 and barnase both show multiple steps in their folding mechanisms. Initial studies showed 2-state folding under equilibrium conditions and multi-state folding under kinetic conditions. However, later studies showed that folding mechanisms for both T1 and barnase included at least one phase that was due to a rate-limiting proline isomerization reaction. In addition, T1 demonstrated multiple unfolded intermediates that involved a rate-limiting proline isomerization reaction. Barnase showed two intermediates, one of which was a rate-limiting proline isomerization reaction. Interestingly, RNase Sa has 6 proline residues in the

trans isomer state and showed no evidence of a rate-limiting proline isomerization step. This implies that proline isomerization is not rate-limiting in the folding of RNase Sa.

The folding of WT* RNase Sa was also observed at low pH under both equilibrium and kinetic conditions. Experiments were performed at pH 3 to provide more evidence that the single site charge reversal of Asp17 was a key component to the results observed at neutral pH. At pH 3, the difference between WT* and WT*(D17R) is a neutral charge for WT* and a single positive charge for WT*(D17R) at position 17. Equilibrium denaturation at pH 3 showed that WT* and WT*(D17R) unfolded in a similar fashion (Figure 7). Stability values calculated in the absence of denaturant were within 0.3 kcal/mol of each other (Table 1), demonstrating that the protein stabilities were more similar when the negatively charged side chain of Asp17 is protonated. Figure 12 shows that WT* folding and unfolding kinetics at pH 3 occur at lower denaturant concentrations as expected. However, a more complicated kinetic mechanism exists under these conditions. The mechanism for folding at pH 3 involved a stable intermediate like at pH 7, but includes an additional step as evidenced by the appearance of a third phase at low denaturant concentrations (Figure 12). This new third phase was not seen at pH 7, and encompassed a very small fraction of the entire reaction amplitude (<10%) shown in Figure 13. This intermediate became increasingly unstable as urea became more concentrated and above 1.4 M was undetectable.

WT*(D17R) RNase Sa showed a similar folding pattern at pH 7 to WT* RNase Sa. Two refolding phases and one unfolding phase were seen. The unfolding rate constant was ten times faster for WT*(D17R) than WT*, which is shown by a positive shift of the unfolding limb of WT* RNase Sa. This is consistent with the proposal of Pace et al. (Pace et al. 2000) in which the electrostatic interactions were proposed to be more significant in the denatured state ensemble than the native state.

Folding of WT*(D17R) RNase Sa was also observed at low pH under the same conditions as WT*. Figure 12 shows that WT* unfolds more readily at pH 3 than at pH 7, as expected. However, a more complicated kinetic mechanism exists at pH 3. The mechanism for folding at pH 3 involved a stable intermediate like at pH 7, but includes an additional step as evidenced by the appearance of a third phase at low denaturant concentrations (Figure 12). This new third phase was not seen at pH 7, and encompassed a very small fraction of the entire reaction amplitude (<10%). This intermediate became increasingly unstable as urea became more concentrated and above 1.4 M was undetectable. The rate constants of unfolding and folding were not calculated for WT* and WT*(D17R). However, it is clear that both variants of RNase Sa in this study folded similarly as shown by overlapping or near overlapping limbs of the folding and unfolding limbs.

The nature of this additional phase at low pH is unclear and will require additional investigation. Whether this intermediate is on pathway, off pathway, or is an additional unfolded form of RNase Sa is not known. However, the objective

of showing that at pH 3 WT* and WT*(D17R) have more similar folding and unfolding behavior than at pH 7 was acheived.

A mechanism that is consistent with the data for folding and unfolding of WT* and WT*(D17R) at pH 7 is shown in Figure 14. Since the slopes of the refolding and unfolding limbs of the chevron plot are non-zero, the stability of the intermediate is dependent on solvent conditions. An intermediate that is independent of solvent conditions, such as proline isomerization, would show a limb with a zero slope. Therefore, an intermediate involving a rate-limiting proline isomerization is not required in this mechanism. In the mechanism of Figure 14, the refolding step of D ↔ I is fast and corresponds to the faster phase observed in Figure 9. The refolding step of I ↔ N corresponds to the slow step of Figure 9. Unfolding shows only one phase because the intermediate is unstable at the high denaturant concentrations necessary to unfold the native state.

FIGURE 14: Proposed folding mechanism of RNase Sa. D = denatured state; I = intermediate; N = native state.

The kinetic folding and unfolding results reported in the study at pH 7 can be represented by two different models (Figure 15). The energy diagram in Figure 15A represents one model, in which both the denatured state and the transition state are stabilized as shown by the decrease in free energy (ΔG). This shows that the difference in free energy between the denatured state and transition state of the mutant is equal to that of WT* RNase Sa. However, the

difference in free energy between the native state and the transition state of the charge-reversed mutant is not the same as the WT*. Thus, any detectable difference in kinetic rate constants of WT* and WT*(D17R) will only be seen in the unfolding reactions.

The second possible model that is consistent with the kinetic data is represented in Figure 15B. In this model, there is no stabilization of either the denatured state or the transition state of WT*(D17R) compared to WT*. However, this model proposes a destabilization of only the native state, which should give similar kinetic results to the previous model. Thus, as with the first model, the only difference in rate constants should be detected in the unfolding rate constant.

Although both models seem to fit the data in accordance to the chevron plot developed for the folding kinetics at pH 7, the first model, as shown in Figure 15A, is more consistent with the equilibrium results. The findings by Pace et al. (Pace et al. 2000) that D17K is a destabilizing mutant, suggests that an expected stabilizing electrostatic interaction introduced by the charge reversal, contributes more to the stability of the denatured state. If this interaction had contributed more to the stability of the native state, then the overall effect would have been an increase in overall stability for WT*(D17R), the opposite of what was discovered for the corresponding variant of RNase Sa (D17K).

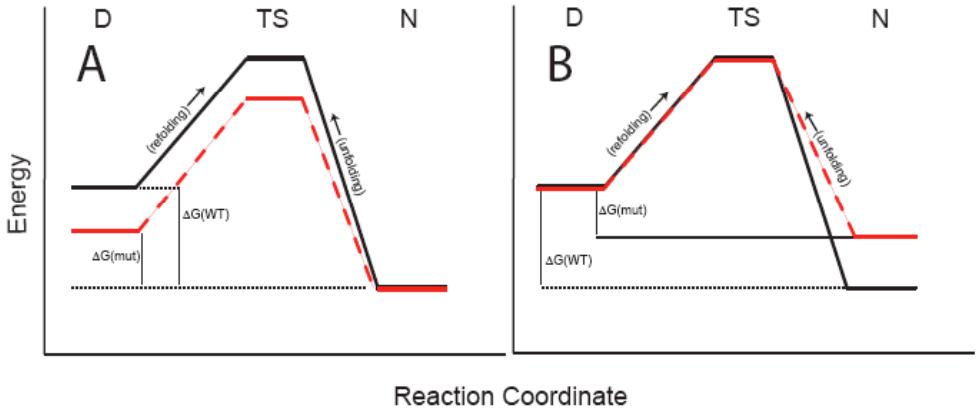

FIGURE 15: Possible energy diagram models based on kinetic data at pH 7. Solid line refers to WT* RNase Sa. Dashed line refers to WT*(D17R) RNase Sa (mut). Energy diagram models show (A) decreased free energy in both the denatured state and the transition state or (B) decreased free enegy ion the native state only due to the effect of the charge reversal. D represents the denatured state, TS represents the transition state and N represents the native state of the proteins.

MATERIALS AND METHODS

Oligonucleotides

Oligonucleotides were made on the 200 nanomole scale by the Gene Technologies Laboratory, Texas A&M University (College Station, Texas) and were used without further purification. Oligonucleotides used for the construction, mutagenesis and sequencing of DNA used are shown in Table 3. Concentration of oligonucleotide stocks were measured on a Gilford Model 250 Spectrophotometer using a 1 cm cuvette and an absorption coefficient for single-stranded DNA of 0.05 mg^{-1} ml cm^{-1}.

TABLE 3: Primers used for generating WT* RNase Sa in the tryptophan background (Y81W) and WT*(D17R) RNase Sa in the tryptophan background (D17R/Y81W). The + and – signs indicate to directionality.

Oligo (Primer)	Sequence
D17R+	5’ –CCGGAAGCTACCCGTACCCTGAACC-3’
D17R-	5’ -GGTTCAGGGTACGGGTAGCTTCCGG-3’
Y81W+	5’ -CAGGAAGACTACTGGACCGGTGACCAC-3’
Y81W-	5’ -GTGGTCACCGGTCCAGTAGTCTTCCTG-3’

Site-Directed Mutagenesis

The MQ cells were prepared and made competent, and the plasmid DNA was prepared as previously described (Hebert et al. 1997). Variants of RNase Sa were made using the four primer polymerase chain reaction (PCR) overlapping extension technique (Ho et al. 1989). Three separate reactions were needed for each variant. The first and second reactions produced the 5’ and 3’ ends of the gene and incorporated a mutated primer in each. The final reaction

resulted in the complete amplification of the altered sequence. 5 pmol of primer, 10 ng pEH100, 200 mM dNTPs, and 2.5 U Vent polymerase were included in a 100ml reaction volume for PCR. The thermal cycler profile was 94^{o}C (2.5 minutes) for 1 cycle, followed by 25 cycles of 94^{o}C (0.5 minutes), 68^{o}C (0.5 minutes), and 72^{o}C (0.5 minutes). Finally, there was a 5.0 minute extension period at 72^{o}C. Samples were frozen at -20^{o}C until needed. PCR products were analyzed by running 5 ml of the reaction on a 1.5 or 2% agarose gel (0.5X TBE, 0.25 mg/ml ethidium bromide). The final PCR product from the mutagenesis reaction was purified using a Qiagen PCR Purification Kit.

The purified PCR product was digested first with *Xba*I and then precipitated with 95% ethanol, *d*H_2O, 7.5 M ammonium acetate, and $MgCl_2$. The PCR product was then digested with *Eco*RI and precipitated again the same way. This purified vector was used in the ligation of mutated phoA-RNase Sa gene cassette recreating pEH100 with the desired mutation. Ligated vector was transformed into competent MQ cells and assumed variants were screened using DNA sequencing. The protein was then purified as described previously with minor modifications (Hebert et al. 1997).

RNase Sa Expression and Purification

For each purification, a freshly transformed stock of *E. coli* MQ cells carrying the wild-type or variant RNase Sa vector was prepared. Freshly transformed cells were grown overnight in 50 ml of LB medium, then diluted 1:10 into 500 ml of Terrific broth. This culture was grown at 30°C to an OD_{600} of 0.6

and subsequently diluted into 10.5 L of terrific broth medium in an 11 L benchtop fermentor (New Brunswick Scientific, Inc., Model 19). The culture was shaken at 350 rpm and aerated with pressurized air at 12 L per minute filtered through an Acro 50 PTFE filter. Growth was continued at 30°C to an OD_{600} of 0.6. At this time, production of RNase Sa expression was induced by the addition of IPTG to a final concentration of 0.1mM for pEH100 vectors. An additional aliquot of ampicillin (25 mg/ml) was also added at this time. Cultures were grown an additional 12 hours before cells were harvested.

RNase Sa was released from the periplasmic space of *E. coli* MQ cells using an osmotic shock treatment. Cells were harvested in a Beckman JS-4.2 rotor at 4,000 rpm for 25 minutes. Cell pellets were resuspended by vigorous shaking in 1800 ml of 20% sucrose, 15 mM Tris pH 7.4, 3 mM Na_2EDTA and transferred to GSA bottles. After centrifugation in a Sorvall GSA rotor at 10,000 rpm for 30 minutes at 4°C, the supernatant was saved and the cell pellets resuspended rapidly by vigorous shaking in 2000 ml of 15 mM Tris pH 7.4, 3 mM Na_2EDTA. After incubation for 20 minutes on ice, cells were pelleted in a Sorvall GSA rotor as before, and this supernatant was added to the first supernatant. The combined supernatants (4000 ml of periplasmic fraction) were acidified by adding 10.8 g Na_2-succinate and 18.8 g succinic acid (final concentrations: 20 mM sodium/50 mM succinate). The final pH was adjusted to 3.25 with concentrated HCl and any precipitate formed was removed by centrifugation in a Sorvall GSA rotor at 10,000 rpm for 20 minutes at 4°C.

Cation exchange chromatography was performed using a SP-Sephadex C25 resin (4.4 x 29 cm: ~450 ml total bed volume) was pre-equilibrated with 3 L of 20 mM sodium/50 mM succinate buffer pH 3.25. The acid precipitated supernatant was loaded at a flow rate of 6.0 ml min^{-1}. After loading, the column was washed with 2 L of the low pH buffer. Elution was performed using a pH gradient from pH 3.25 to pH 6.0 in succinate buffer using a total volume of 2 L. Fraction volumes of 18 ml were collected. All cation exchange chromatography runs were performed at room temperature. Fractions containing RNase activity were pooled and freeze dried.

Enzymatic activity for RNase Sa was measured using the method involving a Toluidine Blue O RNase assay plate (Korn et al. 2001). A small hole is bored into the assay plate sufficient for a 5μl aliquot of solution containing RNase Sa. The plate was incubated for approximately 20 minutes at 30°C. Positive activity showed a visible pinkish purple color around the hole.

The freeze-dried RNase Sa sample from the ion exchange step was dissolved in a solution containing 2-5 ml of 2 M Tris pH 10.5 and 20 ml of 50 mM ammonium bicarbonate buffer (final pH ~7.0). The sample was loaded on a 4.8 x 110 cm Sephadex G-50 column and eluted with 50mM ammonium bicarbonate buffer pH 7.0. All G-50 runs were performed at room temperature. Fraction volumes of 12 ml were collected. Absorbance at 278 nm (tryptophan+tyrosine), 251 nm (nucleic acids), and 330 nm (particulate scatter) were measured to verify protein concentration and purity from cellular RNA. The final purified protein was lyophilized for storage.

Protein Gel Analysis

Protein purity was examined by running the isolated proteins on Bio-Rad 4-20% Tricine-HCl SDS-PAGE Ready Gel. Gels were stained using standard Coomassie Brilliant Blue R-250.

Preparation of Stock Solutions

Urea stock solutions were prepared by weight, and the molarity of the solutions was calculated using the equation below (Kawahara and Tanford 1966):

$$M = 117.66(\Delta N) + 29.753(\Delta N)^2 + 185.56(\Delta N)^3 \quad (6)$$

where ΔN is the difference between the refractive indices of the denaturant and buffer solutions. All refractive indices were measured with an American Optical Abbe refractometer. Urea stock solutions were used within 72 hours after preparation.

Protein concentrations of RNase Sa solutions were determined spectrophotometrically using a Gilford Model 250 spectrophotometer. The molar absorption coefficient of ε_{280} = 12045 M^{-1} cm^{-1} was used for wild-type RNase Sa (Hebert et al. 1997). For the tyrosine to tryptophan (Y81W) variant, the molar absorption coefficients, ε_{280} = 16055 M^{-1} cm^{-1}. The error in determining the protein concentration using a predicted extinction coefficient is ~3.8% (Pace et al. 1995).

Urea Denaturation Studies

The conformational stability of WT* RNase Sa and the charge-reversal variant was determined using urea denaturation as monitored by circular dichroism spectroscopy and fluorescence spectroscopy with an Aviv 62DS or Aviv 202SF spectropolarimeter, respectively. Protein stock solutions were prepared in 30mM MOPS at pH 7.0 and 30 mM glycine at pH 3. Protein concentrations in the sample cell were ~6 μM. The steady-state stability experiments of the WT* and WT*(D17R) were determined using urea denaturation. A sample cuvette holding approximately 2.0 ml of protein in either 30 mM MOPS (pH 7) or 30 mM glycine (pH 3) was prepared. A 10 ml volumetric flask holding 10 M urea (ICN Biomedicals Inc., Aurora, OH) and a 10X dilution of protein sample was prepared and titrated into the sample cuvette at 25°C. Samples were mixed by a rotary stir bar and allowed to equilibrate prior to data acquisition for each denaturation curve. Each sample cuvette and flask of titrant contained the same concentration of protein for each variant.

Analysis of the denaturation curves was performed using the two-state unfolding model and the linear extrapolation method. These two methods were combined into a single equation to describe the shape of the denaturation curve (Santoro and Bolen 1988),

$$y = \left\{\left(y_f + b_f[D]\right) + \left(y_u + b_u[D]\right)\exp\left[(m)(D - C_{mid})/RT\right]\right\} \Big/ \left\{1 + \exp\left[(m)(D - C_{mid})/RT\right]\right\} \quad (7)$$

where, y_f = slope of pre-transition baseline; b_f = y-intercept of pre-transition baseline; y_u = slope of post-transition baseline; b_u = y-intercept of post-transition baseline; m = m-value or slope of the folding transition curve; C_{mid} = midpoint of folding transition curve, and D = denaturant concentration.

Urea concentrations were determined using refractive index measurements (Pace 1986; Pace and Shaw 2000). A thorough explanation of the methods used to analyze the solvent denaturation curves has been previously described (Becktel and Schellman 1987; Nicholson and Scholtz 1996; Pace and Scholtz 1997). Briefly, the unfolding curves were fit by an equation derived from the linear extrapolation method (LEM) (Pace and Scholtz 1997; Pace and Shaw 2000).

Kinetic Folding Studies

All stopped-flow fluorescence measurements were performed at 25 °C and at the indicated pH. RNase Sa (0.6 mg/ml) in denaturant was rapidly mixed to give a 6-fold dilution in 30 mM MOPS at pH 7.0 and 30 mM glycine at pH 3.0. Unfolding kinetic reactions that had rates of > 0.01 s^{-1} were performed by a manual mixing technique using a PTI spectrofluorimeter. RNase Sa was rapidly mixed and diluted 10X to give a final concentration of 0.06mg/ml. Unfolding progress curves were analyzed and fit by an appropriate exponential function using Pro Fit and Kaleidagraph analytical software. The refolding reactions were performed by diluting RNase Sa (0.6 mg/ml) in buffered urea 6-fold into 30mM MOPS at pH 7.0 or 30mM glycine at pH 3.0, to initiate refolding. Refolding progress curves were analyzed and fit by a double exponential function using Pi-

star software. All kinetic rate constants were analyzed to generate a chevron plot by fitting the data to the following equation:

$$\ln\left(k_{obs}\right) = \ln\left[k_f\left(H_2O\right)\exp\left(-m_f\left[D\right]/RT\right) + k_u\left(H_2O\right)\exp\left(m_u\left[D\right]/RT\right)\right] \qquad (8)$$

where k_{obs} is the observed rate constant, k_f and k_u are the refolding and unfolding rate constants, respectively, and R is the gas constant (1.987 cal mol^{-1} K^{-1}).

SUMMARY

This study describes the overall folding kinetic behavior for WT* RNase Sa. Additional information elucidated the mechanism of the charge-reversed side chain of Asp17 on the folding of RNase Sa. This study has resulted in the following conclusions. First, RNase Sa has at least a three-state folding mechanism, which was detected by kinetics. The results do not show evidence for rate-limiting proline isomerization reaction but supports a stable intermediate through which the enzyme folds toward the native state. Second, the electrostatic interaction introduced by the charge-reversal contributes more to the stability of the denatured state than in the native state. This is represented by the increase in the unfolding rate constant (Table 2) for the charge-reversal. Third, WT*(D17R) is characterized as a mixed mutant as defined by Matthews (Matthews 1987). Such a mutant displays equilibrium and kinetic effects. Under equilibrium conditions, WT*(D17R) has a lower stability than WT*. Kinetically, the charge-reversal unfolds nearly one order of magnitude faster than WT* RNase Sa but the refolding rate was unaffected. To our knowledge, this is the first demonstration that a favorable electrostatic interaction in the denatured state ensemble has been shown to influence the unfolding kinetics of a protein.

REFERENCES

Akiyama, S., Takahashi, S., Ishimori, K., and Morishima, I. 2000. Stepwise formation of alpha-helices during cytochrome c folding. *Nat Struct Biol* **7:** 514-520.

Alston, R.W. 1999. Characterization of four single-site tryptophan variants of Ribonuclease Sa. In *Biochemistry and Biophysics*, pp. 77. Texas A&M University, College Station, USA.

Alston, R.W. 2004. Contribution of Single Tryptophan Residues to the Fluorescence and Stability of Ribonuclease Sa. *Biophysical Journal* **87:** 1-12.

Anfinsen, C.B. 1973. Principles that Govern the Folding of Protein Chains. *Science* **181:** 223-230.

Becktel, W.J., and Schellman, J.A. 1987. Protein stability curves. *Biopolymers* **26:** 1859-1877.

Chen, B.L., Baase, W.A., Nicholson, H., and Schellman, J.A. 1992. Folding kinetics of T4 lysozyme and nine mutants at 12 degrees C. *Biochemistry* **31:** 1464-1476.

Daggett, V., and Fersht, A.R. 2003. The Present View of the mechanism of protein folding. *Nat Rev Mol Cell Biol* **4:** 497-502.

Dill, K.A., and Shortle, D. 1991. Denatured states of proteins. *Annu Rev Biochem* **60:** 795-825.

Fersht, A.R. 1999. *Structure and Mechanism in Protein Science: A Guide to Enzyme Catalysis and Protein Folding*. W. H. Freeman & Co.

Fersht, A.R. 2000. A kinetically significant intermediate in the folding of barnase. *Proc Natl Acad Sci USA* **97:** 14121-14126.

Grimsley, G., Shaw, K., Fee, L., Alston, R., Huyghues-Despointes, B., Thurlkill, R., Scholtz, J., and Pace, C. 1999. Increasing protein stability by altering long-range coulombic interactions. *Protein Sci* **8:** 1843-1849.

Hebert, E.J., Giletto, A., Sevcik, J., Urbanikova, L., Wilson, K.S., Dauter, Z., and Pace, C.N. 1998. Contribution of conserved asparagine to the conformational stability of ribonucleases Sa, Ba, and T1. *Biochemistry* **37:** 16192-16200.

Hebert, E.J., Grimsley, G.R., Hartley, R.W., Horn, G., Schell, D., Garcia, S., Both, V., Sevcik, J., and Pace, C.N. 1997. Purification of Ribonucleases Sa, Sa2, and Sa3 after Expression inEscherichia coli. *Protein Expression and Purification* **11:** 162-168.

Hill, C., Dodson, G., Heinemann, U., Saenger, W., Mitsui, Y., Nakamura, K., Borisov, S., Tischenko, G., Polyakov, K., and Pavlovsky, S. 1983. The structural and sequence homology of a family of microbial ribonucleases. *Trends Biochem Sci* **8:** 364-369.

Ho, S.N., Hunt, H.D., Horton, R.M., Pullen, J.K., and Pease, L.R. 1989. Site-directed mutagenesis by overlap extension using the polymerase chain reaction. *Gene* **77:** 51-59.

Hoang, L., Bedard, S., Krishna, M.M.G., Lin, Y., and Englander, S.W. 2002. Cytochrome c folding pathway: Kinetic native-state hydrogen exchange. *Proc Natl Acad Sci USA* **99:** 12173-12178.

Ilinskaya, O.N., Dreyer, F., Mitkevich, V.A., Shaw, K.L., Pace, C.N., and Makarov, A.A. 2002. Changing the net charge from negative to positive makes ribonuclease Sa cytotoxic. *Protein Sci* **11:** 2522-2525.

Kawahara, K., and Tanford, C. 1966. Viscosity and density of aqueous solutions of urea and guanidine hydrochloride. *J Biol Chem* **241:** 3228-3232.

Kazmirski, S.L., Wong, K.-B., Freund, S.M.V., Tan, Y.-J., Fersht, A.R., and Daggett, V. 2001. Protein folding from a highly disordered denatured state: The folding pathway of chymotrypsin inhibitor 2 at atomic resolution. *Proc Natl Acad Sci USA* **98:** 4349-4354.

Khan, F., Chuang, J.I., Gianni, S., and Fersht, A.R. 2003. The kinetic pathway of folding of barnase. *J Mol Biol* **333:** 169-186.

Korn, K., Greiner-Stoffele, T., and Hahn, U. 2001. Ribonuclease assays utilizing toluidine blue indicator plates, methylene blue, or fluorescence correlation spectroscopy. *Methods Enzymol* **341:** 142-153.

Kraulis, P.J. 1991. MOLSCRIPT: A program to produce both detailed and schematic plots of protein structures. *J Appl Crystallogr* **24:** 946-950.

Laurents, D.V., Huyghues-Despointes, B.M., Bruix, M., Thurlkill, R.L., Schell, D., Newsom, S., Grimsley, G.R., Shaw, K.L., Trevino, S., Rico, M., et al. 2003. Charge-charge interactions are key determinants of the pK values of ionizable groups in ribonuclease Sa (pI=3.5) and a basic variant (pI=10.2). *J Mol Biol* **325:** 1077-1092.

Levinthal, C. 1969. How to Fold Graciously. In *Mossbauer Spectroscopy in Biological Systems*. (eds. I. Monticello, P. Debrunner, J. Tsibris, and E. Munck), pp. 22-24. Univ. of Illinois Press, Urbana, USA.

Matouschek, A., Matthews, J.M., Johnson, C.M., and Fersht, A.R. 1994. Extrapolation to water of kinetic and equilibrium data for the unfolding of barnase in urea solutions. *Protein Eng* **7:** 1089-1095.

Matthews, C.R. 1987. Effect of point mutations on the folding of globular proteins. *Methods Enzymol* **154:** 498-511.

Mayr, L.M., Landt, O., Hahn, U., and Schmid, F.X. 1993b. Stability and folding kinetics of ribonuclease T1 are strongly altered by the replacement of cis-proline 39 with alanine. *J Mol Biol* **231:** 897-912.

Mayr, L.M., Odefey, C., Schutkowski, M., and Schmid, F.X. 1996. Kinetic analysis of the unfolding and refolding of ribonuclease T1 by a stopped-flow double-mixing technique. *Biochemistry* **35:** 5550-5561.

Mayr, L.M., and Schmid, F.X. 1993. Kinetic models for unfolding and refolding of ribonuclease T1 with substitution of cis-proline 39 by alanine. *J Mol Biol* **231:** 913-926.

Myers, J.K., Pace, C.N., and Scholtz, J.M. 1995. Denaturant m values and heat capacity changes: relation to changes in accessible surface areas of protein unfolding. *Protein Sci* **4:** 2138-2148.

Nicholson, E.M., and Scholtz, J.M. 1996. Conformational stability of the Escherichia coli HPr protein: test of the linear extrapolation method and a thermodynamic characterization of cold denaturation. *Biochemistry* **35:** 11369-11378.

Pace, C., Alston, R., and Shaw, K. 2000. Charge-charge interactions influence the denatured state ensemble and contribute to protein stability. *Protein Sci* **9:** 1395-1398.

Pace, C.N. 1986. Determination and analysis of urea and guanidine hydrochloride denaturation curves. *Methods Enzymol* **131:** 266-280.

Pace, C.N., Hebert, E.J., Shaw, K.L., Schell, D., Both, V., Krajcikova, D., Sevcik, J., Wilson, K.S., Dauter, Z., Hartley, R.W., et al. 1998. Conformational stability and thermodynamics of folding of ribonucleases Sa, Sa2 and Sa3. *J Mol Biol* **279:** 271-286.

Pace, C.N., Horn, G., Hebert, E.J., Bechert, J., Shaw, K., Urbanikova, L., Scholtz, J.M., and Sevcik, J. 2001. Tyrosine hydrogen bonds make a large contribution to protein stability. *J Mol Biol* **312:** 393-404.

Pace, C.N., and Scholtz, J.M. 1997. Measuring the Conformational Stability of a Protein. In *Protein Structure: A Practical Approach*. (ed. T.E. Creighton), pp. 299-321. IRL Press, Oxford, UK.

Pace, C.N., and Shaw, K.L. 2000. Linear Extrapolation Method of Analyzing Solvent Denaturation Curves. *Proteins: Structure, Function, and Genetics* **41:** 1-7.

Pace, C.N., Vajdos, F., Fee, L., Grimsley, G., and Gray, T. 1995. How to measure and predict the molar absorption coefficient of a protein. *Protein Sci* **4:** 2411-2423.

Rang, H.P., Dale, M.M., Ritter, J.M., and Gardner, P. 2001. *Pharmacology*, 4th edition ed. Churchill Livingstone, New York, USA pp. 839.

Rosenburg, H.F., Dyer, K.D., Tiffany, H.L., and Gonzalez, M. 1995. Rapid evolution of a unique family of primate ribonuclease genes. *Nature Genet* **10:** 219-223.

Santoro, M.M., and Bolen, D.W. 1988. Unfolding free energy changes determined by the linear extrapolation method. 1. Unfolding of phenylmethanesulfonyl alpha-chymotrypsin using different denaturants. *Biochemistry* **27:** 8063-8068.

Schell, D. 2003. Computational and Experimental Investigatiopn of Forces in Protein Folding. In *Biochemistry and Biophysics*, pp. 140. Texas A&M University, College Station, USA.

Serrano, L., Matouschek, A., and Fersht, A.R. 1992. The folding of an enzyme. VI. The folding pathway of barnase: comparison with theoretical models. *J Mol Biol* **224:** 847-859.

Sevcik, J., Dauter, Z., Lamzin, V.S., and Wilson, K. 1996. Ribonuclease from Streptomyces aureofaciens at atomic resolution. *Acta Crystallogr* **D52:** 327-344.

Sevcik, J., Dodson, E.J., and Dodson, G.G. 1991. Determination and restrained least-squares refinement of the structures of ribonuclease Sa and its complex with 3'-guanylic acid at 1.8 A resolution. *Acta Crystallogr* **B47:** 240-253.

Sevcik, J., Hill, C.P., Dauter, Z., and Wilson, K.S. 1993a. Complex of ribonuclease from Streptomyces aureofaciens with 2'-GMP at 1.7 Å resolution. *Acta Crystallogr* **D49:** 257-271.

Sevcik, J., Lamzin, V.S., Dauter, Z., and Wilson, K.S. 2002. Atomic resolution data reveal flexibility in the structure of RNase Sa. *Acta Crystallogr* **D58:** 1307-1313.

Sevcik, J., Sanishvili, R.G., Pavlovsky, A.G., and Polyakov, K.M. 1990. Comparison of active sites of some microbial ribonucleases: structural basis for guanylic specificity. *Trends Biochem Sci* **15:** 158-162.

Sevcik, J., Zegers, I., Wyns, L., Dauter, Z., and Wilson, K.S. 1993. Complex of ribonuclease Sa with a cyclic nucleotide and a proposed model for the reaction intermediate. *Eur J Biochem* **216:** 301-305.

Shaw, K.L., Grimsley, G.R., Yakovlev, G.I., Makarov, A.A., and Pace, C.N. 2001. The effect of net charge on the solubility, activity, and stability of ribonuclease Sa. *Protein Sci* **10:** 1206-1215.

Tanford, C., Kawahara, K., and Lapanje, S. 1966. Proteins in 6-M guanidine hydrochloride. Demonstration of random coil behavior. *J Biol Chem* **241:** 1921-1923.

Wong, K.-B., Clarke, J., Bond, C.J., Neira, J.L., Freund, S.M.V., Fersht, A.R., and Daggett, V. 2000. Towards a Complete Description of the Structural and Dynamic Properties of the Denatured State of Barnase and the Role of Residual Structure in Folding,. *J Mol Biol* **296:** 1257-1282.

Yakovlev, G.I., Mitkevich, V.A., Shaw, K.L., Trevino, S., Newsom, S., Pace, C.N., and Makarov, A.A. 2003. Contribution of active site residues to the activity and thermal stability of ribonuclease Sa. *Protein Sci* **12:** 2367-2373.

Yeh, S.R., and Rousseau, D.L. 2000. Hierarchical folding of cytochrome c. *Nat Struct Biol* **7:** 443-445.

VITA

Jared Matthew Trefethen

708 Aster Dr.

College Station, TX 77845

Jared Matthew Trefethen was born in Bellevue, Washington in 1975. After graduating from Newbury Park High School of Newbury Park, California in 1994, he served a mission for The Church of Jesus Christ of Latter-day Saints through the end of 1996. He married Emily Renae Brems in 1997, and a year later his first child, Madeline Jayne, was born. He graduated thereafter with a Bachelor of Science degree in Biochemistry from The University of California, Los Angeles in September of 2002, only months after his second child, Naomi Katherine, was born. He then enrolled in Texas A&M University, in College Station, Texas and has completed the requirements for a Master of Science degree in Biochemistry. He will be awarded the degree in December of 2004